JACS
JOURNAL OF THE AMERICAN CHEMICAL SOCIETY
Article
Cite This: J. Am. Chem. Soc. 2019, 141, 20318−20324
pubs.acs.org/JACS

Critical Role of Tricyclic Bridges Including Neighboring Rings for Understanding Raman Spectra of Zeolites

Tongkun Wang,[†,∥] Song Luo,[‡,∥] Geoffrey A. Tompsett,[§] Michael T. Timko,[§] Wei Fan,*[,‡] and Scott M. Auerbach*[,†,‡]

[†]Department of Chemistry and [‡]Department of Chemical Engineering, University of Massachusetts Amherst, Amherst, Massachusetts 01003, United States

[§]Department of Chemical Engineering, Worcester Polytechnic Institute, Worcester, Massachusetts 01609, United States

Supporting Information

ABSTRACT: Raman spectroscopy of network solids such as zeolites is critical for shedding light on collective vibrations of medium-range structures such as rings that exist in crystals and that form during crystallization processes. Despite this importance, assignments of Raman spectra are not completely understood, though it is often assumed that Raman bands can be assigned to individual rings. We report a systematic zeolite synthesis, spectroscopy, and periodic DFT study of several all-silica zeolites to test this assumption and to determine the fundamental structural motifs that explain Raman spectral features. We have discovered from normal-mode analysis that Raman bands can be assigned to tricyclic bridges—three zeolite rings that share a common Si−O−Si bridge. Furthermore, we have found that the vibrational frequency of a given Raman band can be correlated to the smallest ring of its tricyclic bridge and not to the ring that is actually vibrating. Finally, we have discovered a precise anticorrelation between Raman frequency and Si−O−Si angle. These discoveries open new ways to investigate structures of network materials made of corner-sharing tetrahedra and to study crystallization from amorphous gels where structural information is limited.

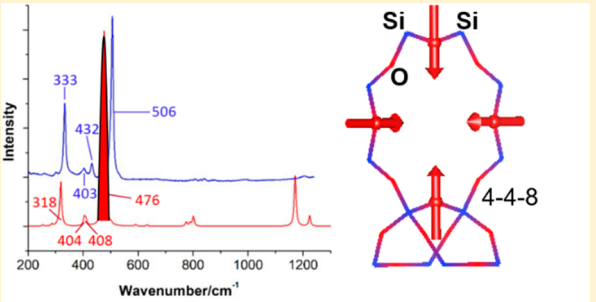

Raman spectra of zeolites explained by tricyclic bridge.

1. INTRODUCTION

Understanding the formation mechanisms of nanoporous catalysts such as zeolites,[1] which can open the door to tailoring materials for advanced applications in catalysis and separations,[2,3] has remained a tantalizing challenge.[4,5] Discovering how zeolites form is complicated by the fact that zeolite precursor structures fall into a nanoscale blind spot—too large for atomic-level and functional group structural analyses by methods like IR and NMR and too disordered for X-ray diffraction—necessitating characterization methods sensitive to medium-range structures such as rings and larger building units.[6,7] Raman spectroscopy[8] has emerged as a powerful tool for probing medium-range structures in a variety of materials including disordered silica,[9] zeolites,[10] MOFs,[11] and zeolite precursor solutions.[12−14] However, despite significant research into the Raman spectra of zeolites,[15−21] the detailed assignments of such Raman spectra are not completely understood, though it is often assumed that Raman bands can be assigned to individual ring structures.[22] For example, Suzuki et al. collected Raman spectra of amorphous gels leading to zeolites VPI-7, sodalite, and ferrierite[23] and concluded that these amorphous gels contain high concentrations of 3-membered rings (3MR), 4MR, and 5MR, respectively, which correspond to rings found in the respective zeolite frameworks. This intriguing result raises a fundamental question: can Raman features really be assigned to individual rings or should they be associated with other, possibly larger building units? We answer this question rigorously through an integrated synthesis, spectroscopy, and periodic DFT modeling study.

The zeolites CHA and LTA [Figure 1a,b] present a fascinating test case, both comprising 4MR, 6MR, and 8MR, though in different arrangements. If assigning Raman features to individual rings were valid, then these zeolites would present essentially identical Raman spectra. Interestingly, previously reported Raman spectra for CHA[24] and LTA[10] differ substantially in the key 200−700 cm^{-1} range associated with framework vibrations, with CHA exhibiting a doublet around 475 cm^{-1} assigned to 4MR vibrations,[24] and LTA showing a singlet around 505 cm^{-1} assigned to the so-called ν_s(T-O-T) mode, the symmetric stretch of T-O-T bridges (T = tetrahedral atom = Si or Al).[10] The simple assignment of Raman features to single ring structures cannot explain this discrepancy. Unfortunately, extracting chemical insights from these Raman spectra is greatly complicated by the fact that these zeolites have different chemical compositions (i.e., Si/Al ratios). Advancing our understanding of nanopore framework vibrations requires a synthesis and Raman spectroscopy study

Received: October 3, 2019
Published: November 28, 2019

DOI: 10.1021/jacs.9b10346
J. Am. Chem. Soc. 2019, 141, 20318−20324

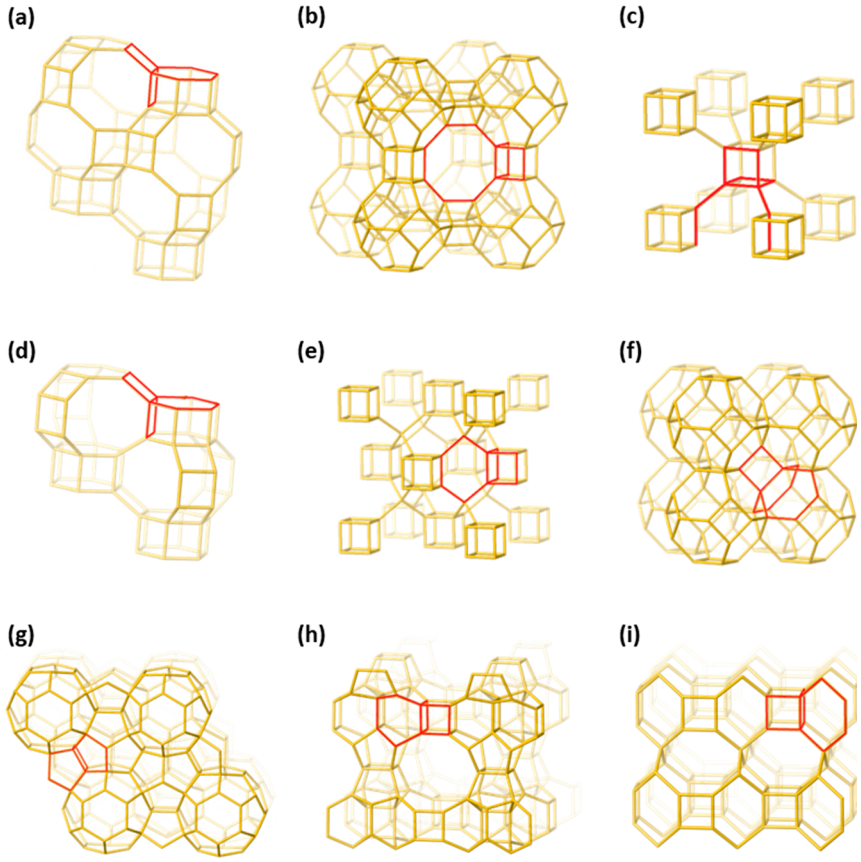

Figure 1. Structures of (a) CHA, (b) LTA, (c) ACO, (d) GME, (e) AST, (f) SOD, (g) DOH, (h) ITH, and (i) ITW. Linkages shown in red provide examples of tricyclic bridges.

on a range of well-defined zeolite frameworks that differ from one another in known, systematic ways, complemented by predictive theory for rigorous assignment of the key Raman features.[25] We report such a study herein, finding that Raman spectra of zeolites can be understood in terms of rings embedded in "tricyclic bridges" as described below.

The remainder of this article is organized as follows: in section 2 we outline the key synthesis, characterization, Raman spectroscopy, and computational DFT methods used in this study with remaining details offered in the Supporting Information; in section 3 we describe the experimental and computational results, and introduce the notion of tricyclic bridges to explain trends in Raman spectra; and in section 4 we offer a summary and concluding remarks.

2. METHODS

2.1. Zeolites Studied. For systematic study of the effects of ring structures on Raman spectra of zeolites, we selected zeolite frameworks based on the following criteria: (i) synthesizable as all-silica materials to remove ambiguities regarding distributions of framework heteroatoms such as Al, and mobile charge-compensating species such as Na; (ii) involving unit cells that are sufficiently small to allow accurate periodic DFT calculations of lattice energy, framework structure, normal modes, and Raman intensities; and (iii) containing 4MRs in various arrangements[26] to allow direct comparisons of Raman features. Figure 1 shows the nine zeolite frameworks studied herein, ranging from the very simple SOD zeolite structure with only 4MR and 6MR to the relatively complicated ITH material with 4MR, 5MR, 6MR, 9MR, and 10MR (see Table S1 for more structural information on these zeolites). We computed DFT-based Raman spectra for each of these nine structures; synthesized all-silica SOD, AST, LTA, CHA, ITW, and ITH zeolites; and measured their Raman spectra to compare with calculations.

2.2. Experimental Methods. Zeolite syntheses were based on previously reported methods (see details in the Supporting Information (SI), section S2.1). All-silica CHA[27] was crystallized using a commercial organic structure-directing agent (OSDA), while the all-silica zeolites AST,[28] ITH,[29] ITW,[30] and LTA[31] were crystallized by fluoride-mediated methods after four specialty OSDAs were synthesized and confirmed by NMR (peak positions reported in SI, section S2.1). All-silica SOD[32] was synthesized by a phase-transformation pathway starting from silicates with double 4MR. All zeolite syntheses were confirmed by X-ray diffraction (XRD) as detailed in SI, sectoion S2.2, by comparing with literature XRD data (shown in SI, Figure S1). Raman spectra were collected on calcined zeolite samples using an XploRa Raman microscope with a 785 nm laser line.

2.3. Computational Methods. Initial structural data for modeling all-silica zeolites ACO, AST, CHA, DOH, GME, LTA, ITH, ITW, and SOD were downloaded from the IZA Web site.[26] All calculations were based on periodic density functional theory (DFT) with plane wave basis sets using the Vienna Ab initio Simulation Package (VASP).[33] We used projector augmented wave pseudopotentials[34,35] and the Perdew–Burke–Ernzerhof (PBE) exchange-correlation functional for structural optimization, normal-mode analysis, and Raman intensity calculations[36] (details are given in the SI, section S3). Normal mode vibrations were visualized and analyzed using the program VESTA,[37] focusing on symmetric stretch [ν_s(T-O-T)] modes of Si–O–Si bridges following the previous work of Dutta et al.[10]

3. RESULTS AND DISCUSSION

3.1. Comparisons between Experimental and Computed Raman Spectra. The measured (blue) and predicted

DOI: 10.1021/jacs.9b10346
J. Am. Chem. Soc. 2019, 141, 20318–20324

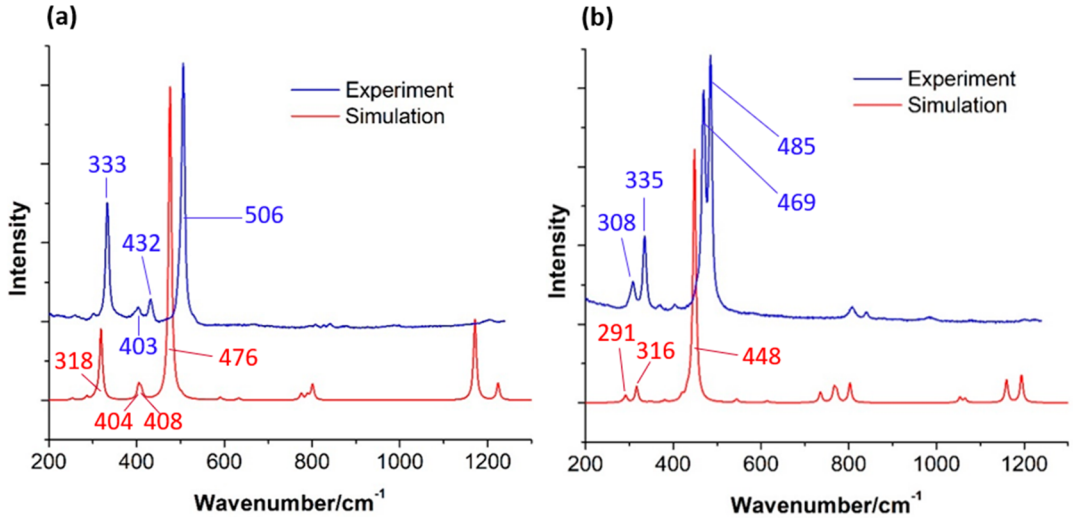

Figure 2. Comparison between experimental and simulated Raman spectra of (a) Si-LTA and (b) Si-CHA.

(red) Raman spectra of LTA and CHA zeolites are shown in Figure 2, panels a (LTA) and b (CHA). The main feature in the experimental LTA spectrum at 506 cm^{-1} corresponds with the band observed at 489 cm^{-1} by Dutta and Del Barco for Na-A;[10] the slight blue shift is expected when replacing Si−O−Al bonds in Na-A with the slightly stiffer Si−O−Si bonds in Si-LTA. The doublet observed for Si-CHA in Figure 2b at about 475 cm^{-1} is characteristic of the CHA structure, as reported in previous work.[24]

Very good agreement between experimental (blue) and computed (red) Raman spectra is clearly visible for both LTA and CHA materials. In particular, Figure 2a,b shows that theory accurately reproduces most patterns in Raman band intensities. The main difference is the missing doublet in the computed CHA spectrum (Figure 2b). There are actually two Raman-active modes predicted by theory for CHA at ∼448 cm^{-1}, but the splitting between these modes is underestimated by normal-mode analysis. Overall the computed frequencies appear to be red-shifted from experiment by about 20−25 cm^{-1}. This red-shift was observed in all of the six zeolites (SOD, AST, LTA, CHA, ITW, and ITH; Raman spectra shown in Figure S3) where direct comparisons are possible, as summarized by the parity plot in Figure 3. A best-fit line through these data gives a slope of 1.02, intercept of 19.6 cm^{-1}, and R^2 = 0.96, indicating a regular pattern of systematic error. Such a red-shift is expected from the PBE density functional, which is known[38,39] to slightly overestimate lattice parameters by about 1% (see the SI, Table S2 for DFT optimized lattice parameters), and hence to slightly underestimate vibrational frequencies. The high degree of agreement between the experimental and simulated Raman spectra allows the assignment of Raman bands to particular vibrational modes in the silica zeolite structures, which can help pinpoint the role of rings in Raman spectra of zeolites.

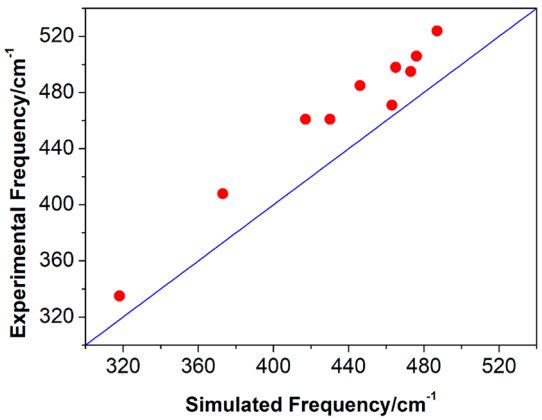

Figure 3. Parity plot comparing experimental and simulated Raman band locations, indicating that theory consistently red-shifts by 20−25 cm^{-1}.

If the Raman spectra were essentially identical for Si-LTA and Si-CHA—two zeolites with the same collection of rings (4MR, 6MR, and 8MR)—it would be justified to assign the bands to individual ring modes. However, while the spectra in Figure 2a,b are similar, they are sufficiently different to necessitate more rigorous assignments that go beyond associating bands to individual 4MR, 6MR, and 8MR. Furthermore, we note that, while Si-SOD contains two different rings (4MR and 6MR), its Raman spectrum exhibits only a single band in the 200−600 cm^{-1} range (Figure S3d), suggesting that a more rigorous assignment is required to determine how 4MR and 6MR conspire in SOD to produce the single band. The previous assignments of the CHA doublet to 4MR vibrations[24] and the LTA singlet to T-O-T bridges[10] were made by comparative and inductive reasoning;[15,16] here we report assignments based on normal-mode analysis by periodic DFT calculations.

3.2. Normal Mode Analysis for LTA. Figure 4 shows the results of normal-mode analysis for Si-LTA. Images of the normal mode eigenvectors for the main LTA feature at 476 cm^{-1} and the smaller band at 318 cm^{-1} are shown in Figure 4a; these reveal ring breathing via oxygen motion in Si−O−Si bridges with surprising patterns. For example, the normal mode for 318 cm^{-1} appears to be an 8MR breathing mode because the normal-mode vectors show displacements in the plane of the 8MR. This would be a surprising and controversial assignment because Raman bands in this frequency range (300−350 cm^{-1}) are typically associated with 6MR vibrations (cf., the CHA band at 335 cm^{-1} assigned to the double-6MR).[24] However, on closer inspection, we see in Figure 4a that only the Si−O−Si bridges that also make up 6MR

DOI: 10.1021/jacs.9b10346
J. Am. Chem. Soc. 2019, 141, 20318−20324

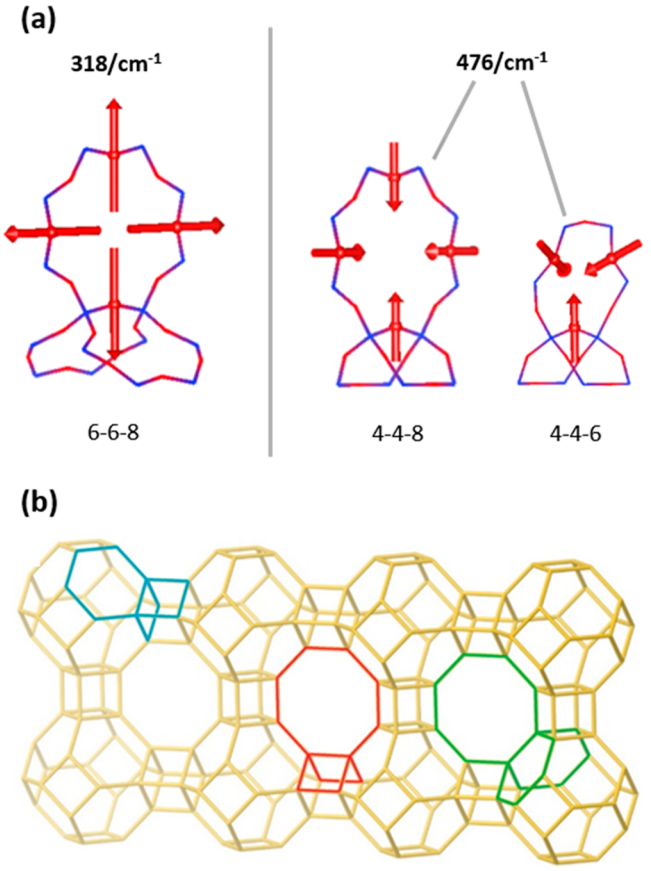

Figure 4. (a) Normal mode eigenvectors computed for LTA vibrations at 318 and 476 cm^{-1}; (b) LTA structure showing three different tricyclic bridges (4−4−6 in blue, 4−4−8 in red, and 6−6−8 in green).

participate in this normal mode. As a second example, the normal mode for 476 cm^{-1} appears to be a mixture of 8MR and 6MR breathing modes (Figure 4a). This would constitute another surprising assignment because Raman bands in this frequency range (450−500 cm^{-1}) are often associated with 4MR motions.[10,24] Then again, on closer inspection, we see that only the Si−O−Si bridges which also make up 4MR contribute to LTA vibration at 476 cm^{-1}. These findings necessitate a new way to understand zeolite structures that takes into account both a given ring structure and its immediate environment.

3.3. Interpretations Using Tricyclic Bridges. The major new insight in this article involves understanding zeolite structure and vibrations in terms of so-called "tricyclic bridges." These are defined as three zeolite rings that share a common Si−O−Si bridge, such as those shown in Figure 4a and highlighted in Figure 4b. Tricyclic bridges are general structural elements of all materials built from corner-sharing tetrahedra, because each bridge (≡T—X—T′≡ where T,T′ = tetrahedral atoms, X = bridge atom) connects to three rings in the network (Figure 4b). Because each tricyclic bridge contains a given ring and its nearby environment, this new notion can help explain the Raman assignments discussed above. In particular, the 8MR breathing mode in Figure 4a at 318 cm^{-1}, a frequency typically associated with 6MR vibrations, is assigned to a tricyclic bridge containing the 8MR and two 6MR. This observation suggests the following general principle: the vibrational frequency of a given Raman band can be correlated to the smallest ring of its tricyclic bridge and not to the ring that is actually vibrating.

We now test this principle on the mixed 6MR/8MR breathing mode in Figure 4a at 476 cm^{-1} − a frequency often associated with 4MR vibrations. This normal mode involves two tricyclic bridges: the first is a 6MR with two 4MR; the second is an 8MR with two 4MR. As such, both tricyclic bridges have 4MR as the smallest ring, which comports with a Raman band at 476 cm^{-1}. Because of the apparent primary importance of the smallest ring in a tricyclic bridge, we name tricyclic bridges in increasing order of ring size. Thus, the normal mode for LTA at 318 cm^{-1} is assigned to a 6−6−8 tricyclic bridge, whereas LTA motion at 476 cm^{-1} is assigned to a mixture of 4−4−6 and 4−4−8 tricyclic bridges. We note that for the LTA structure, the 4−4−6 and 4−4−8 vibrations combine to yield a collective vibration of the double-4MR; below we discuss the generality of this finding. An analysis of the Si−O−Si angle distribution in Si-LTA reveals three distinct angles (Table S1), each corresponding to one of these tricyclic bridges. As such, these three tricyclic bridges account for the distinct structural building blocks of LTA as shown in Figure 4b, as well as the main features of its Raman spectrum.

We have assigned the main features of the Raman spectra in the ring-breathing region for all nine zeolites studied herein, using periodic DFT and normal-mode analysis along with the concept of tricyclic bridges, as described above for LTA. The tricyclic bridge assignments for all main bands are given in Table 1 (see Figure S4 for all relevant tricyclic bridges), along with the corresponding DFT-computed frequencies and Si−O−Si angles from DFT-optimized structures. The conundrum mentioned above for understanding the single Raman band of SOD is resolved by the fact that, although SOD contains 4MR and 6MR, it contains only one unique tricyclic bridge—the 4−6−6 as shown in Table 1. In all cases, the main band is in the 400−500 cm^{-1} region (see Figure 5), consistent with the fact that each main band is assigned to one or more tricyclic bridges with the 4MR as its smallest ring. In most cases, this main band is assigned to a mix of two or more tricyclic bridges, suggesting that the concept of assigning Raman bands to individual rings is overly simplistic.

Table 1. Assignments of Main Raman Bands to Tricyclic Bridges and Their Corresponding Si−O−Si Angles

zeolite	ITH	ACO	LTA	ITW	AST	CHA	GME	SOD	DOH
computed band (cm^{-1})	487	477	476	468	465	448	446	417	408
tricyclic bridge assignment(s)	4−5−5	4−4−8	4−4−6	4−4−5	4−4−6	4−4−6	4−4−6	4−6−6	4−5−5
	4−5−6		4−4−8	4−4−6		4−4−8	4−4−8		
				4−4−8					
Si−O−Si angle[a]	138.5	146.7	147.9	144.5	148.3	148.6	150.1	158.9	162.0

[a]For assignments to several tricyclic bridges, reported Si−O−Si angle is averaged over relevant DFT-optimized angles.

DOI: 10.1021/jacs.9b10346
J. Am. Chem. Soc. 2019, 141, 20318−20324

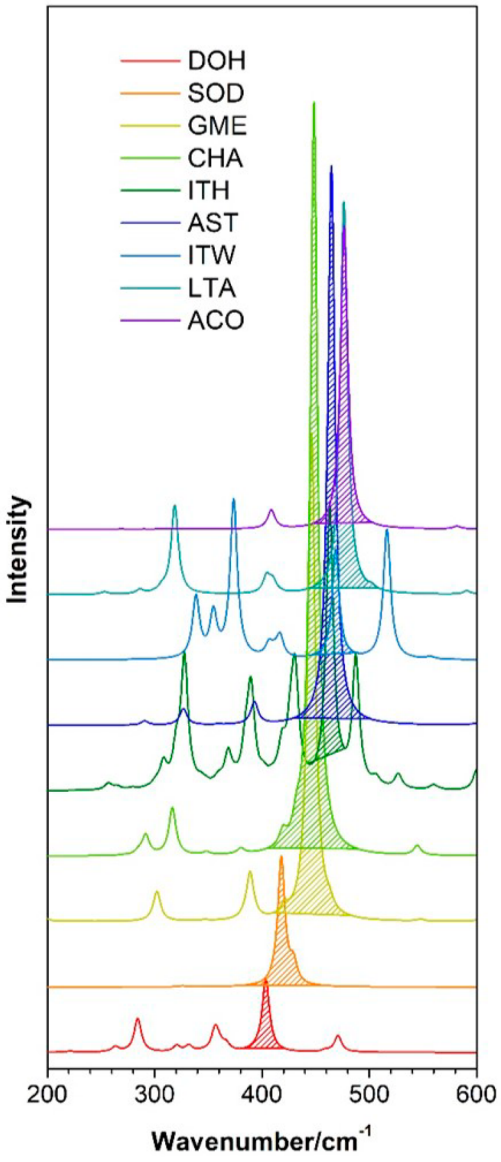

Figure 5. Calculated Raman spectra of all nine zeolites.

It is interesting to connect tricyclic bridges with zeolite collective building units (CBUs) such as the double-4MR, a cubic topology. Five out of the nine zeolites modeled in our work contain the double-4MR; these five zeolites are ITH, ACO, LTA, ITW, and AST, the first five listed in Table 1. In four of these five zeolites (all but ITH), the major Raman band in the 450−500 cm^{-1} range can be thought of as a collective vibration of the corresponding double-4MR, as indicated in Table 1 by the assignments to 4−4−x tricyclic bridges. In the case of zeolite ACO, its double-4MR vibration arises from the motion of only a single type of 4−4−x tricyclic bridge, namely, the 4−4−8 as shown in Table 1. The same is true for zeolite AST and its 4−4−6 bridge. However, zeolites LTA and ITW require several different tricyclic bridges to combine to yield the double-4MR vibration. In general, when a zeolite contains a double-4MR, it also contains 4−4−x tricyclic bridges. However, we caution that that converse of that statement is not true, as evidenced by zeolites CHA and GME in Table 1, both of which contain 4−4−x tricyclic bridges, but neither contains the double-4MR. As such, assigning Raman bands to CBUs in zeolites remains a complex work in progress, while assigning Raman bands to tricyclic bridges emerges naturally from normal-mode analysis.

3.4. Raman Frequency and Si−O−Si Angle. A simple trend arises when we consider the correlation of Raman frequency and Si−O−Si angle, as seen in Table 1. The possibility of such a dependence in the vibrational density of states was first theorized in 1977 for tetrahedral glasses such as silica,[40,41] and then later observed empirically by Dutta et al.[16] in their investigation of Raman spectra for zeolites with a relatively narrow range of angles. Our results put this relationship on a firm ab initio foundation and extend this to a much broader range of angles and framework structures. For Raman features that mix several tricyclic bridges (such as LTA 476 cm^{-1}, mixing 4−4−6 and 4−4−8), Table 1 shows the average Si−O−Si angle (see Table S3 for details on all angles). In almost all cases of tricyclic-bridge mixing, the participating Si−O−Si angles are very similar, which may explain the origin of such mixing.

To underscore our new approach for understanding the Raman spectra of zeolites, we show all the computed Raman spectra for the nine zeolites in Figure 5, which clearly shows the trend in the main band in the 400−500 cm^{-1} region. Band assignment by normal-mode analysis shows that each of these main bands is associated with one or more 4-*x*-*y* tricyclic bridges (see Table 1), where *x* and *y* vary with zeolite structure. Figure 6 shows the correlation of Raman frequency and Si−O−Si angle, with a correlation coefficient of 0.88 over a broad range of angles (24°).

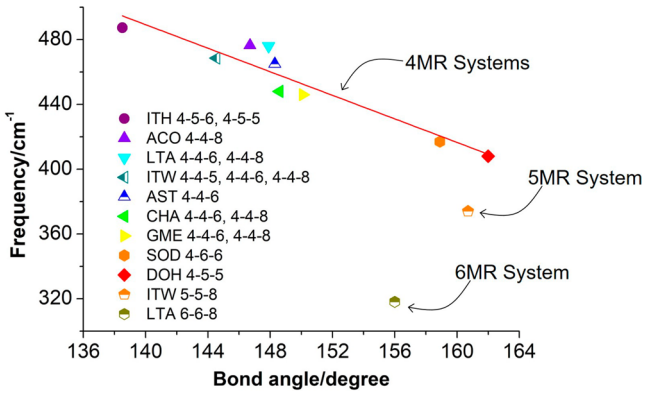

Figure 6. Correlation between computed main-band Raman frequency and Si−O−Si angle in simulation; the slope of the best-fit line is −3.64 and the correlation coefficient (R^2) is 0.88.

Two outliers are included in Figure 6 for illustration purposes: a band for zeolite Si-ITW with a computed frequency of 374 cm^{-1} and a band for Si-LTA at 318 cm^{-1}. Clearly neither of these points falls on the frequency-angle correlation line. These apparent outliers make perfect sense based on our notion of tricyclic bridges. All of the Raman bands that fit the line involve individual 4-−*x*−*y* tricyclic bridges or mixtures thereof, and as such represent a generalized notion of 4MR systems. Instead of assigning Raman bands to individual zeolite rings, we now assign Raman bands to tricyclic bridges and group them together based on the smallest ring in the tricyclic bridge. Figure 6 shows such a grouping for 4-−*x*−*y* tricyclic bridges, arising from our study of several zeolites, all with 4MR. The outlier point for Si-ITW, assigned to a 5−5−8 tricyclic bridge, is predicted to lie on a different correlation line associated with 5-−*x*−*y* tricyclic bridges; we

DOI: 10.1021/jacs.9b10346
J. Am. Chem. Soc. 2019, 141, 20318−20324

will test that prediction in future work by studying a collection of zeolites containing 5MR. Furthermore, the outlier point for Si-LTA (6−6−8) is predicted to lie on a correlation line for 6−x−y tricyclic bridges obtained from studying zeolites with 6MR.

4. CONCLUSIONS

We have engaged in an integrated synthesis, spectroscopy, and periodic DFT modeling study which has shown that assigning features present in the Raman spectra of zeolites to individual rings is overly simplistic. Instead, the new notion of making assignments based on tricyclic bridges is more robust. Such structures are collections of three zeolite rings that have common Si−O−Si (or more generally T-X-T′) bridges. Tricyclic bridges are common elements of all zeolites and all materials built from corner-sharing tetrahedra. By organizing Raman bands according to the smallest ring of their assigned tricyclic bridges, we have shown a strong correlation (for 4MR systems) of Raman vibrational frequency and Si−O−Si angle.

This discovery will be particularly important for investigating crystalline structures of zeolites affected by heteroatoms and organic structure-directing agents, as well as the formation of zeolite crystals from amorphous precursors. Despite the intense effort to understand the fundamental structures participating in zeolite crystallization, the lack of suitable analytical techniques makes atomic-level characterization of zeolite formation processes extremely challenging. Our approach could be used to reinterpret the data of Suzuki et al.,[23] who collected Raman spectra of amorphous gels, in terms of tricyclic bridges and T-O-T′ bond angles present during zeolite formation. Overall, the findings reported herein enhance our ability to use Raman spectroscopy as an analytical tool for investigating zeolite structure and formation, using the new concept of tricyclic bridges.

■ ASSOCIATED CONTENT

Supporting Information

The Supporting Information is available free of charge at https://pubs.acs.org/doi/10.1021/jacs.9b10346.

Structural Information on systems studied; experimental methods; computational methods and convergence tests; X-ray diffraction for all zeolites synthesized; Raman spectra for zeolites; character tables for all zeolites studied; and DFT-optimized coordinates for all zeolites (PDF)

■ AUTHOR INFORMATION

Corresponding Authors

*wfan@engin.umass.edu
*auerbach@umass.edu

ORCID

Wei Fan: 0000-0002-8581-2651
Scott M. Auerbach: 0000-0001-8598-3082

Author Contributions

‖T.W. and S.L. contributed equally to this work.

Notes

The authors declare no competing financial interest.

■ ACKNOWLEDGMENTS

This work was supported by the U.S. Department of Energy, Office of Science, Basic Energy Sciences, Materials Sciences and Engineering Division, under Award No. DE-SC0019170.

■ REFERENCES

(1) Auerbach, S. M.; Karrado, K. A.; Dutta, P. K. *Handbook of Zeolite Science and Technology*. Marcel Dekker: New York, 2003.

(2) Lin, L.-C.; Berger, A. H.; Martin, R. L.; Kim, J.; Swisher, J. A.; Jariwala, K.; Rycroft, C. H.; Bhown, A. S.; Deem, M. W.; Haranczyk, M.; Smit, B. In silico screening of carbon-capture materials. *Nat. Mater.* **2012**, *11*, 633−641.

(3) Davis, M. E. Ordered porous materials for emerging applications. *Nature* **2002**, *417* (6891), 813−821.

(4) Auerbach, S. M.; Fan, W.; Monson, P. A. Modelling the assembly of nanoporous silica materials. *Int. Rev. Phys. Chem.* **2015**, *34* (1), 35−70.

(5) Davis, M. E. Zeolites from a Materials Chemistry Perspective. *Chem. Mater.* **2014**, *26* (1), 239−245.

(6) Cundy, C. S.; Cox, P. A. The hydrothermal synthesis of zeolites: Precursors, intermediates and reaction mechanism. *Microporous Mesoporous Mater.* **2005**, *82* (1−2), 1−78.

(7) Wakihara, T.; Kohara, S.; Sankar, G.; Saito, S.; Sanchez-Sanchez, M.; Overweg, A. R.; Fan, W.; Ogura, M.; Okubo, T. A new approach to the determination of atomic-architecture of amorphous zeolite precursors by high-energy X-ray diffraction technique. *Phys. Chem. Chem. Phys.* **2006**, *8* (2), 224−227.

(8) Opilik, L.; Schmid, T.; Zenobi, R. Modern Raman Imaging: Vibrational Spectroscopy on the Micrometer and Nanometer Scales. *Annu. Rev. Anal. Chem.* **2013**, *6* (1), 379−398.

(9) Geisler, T.; Dohmen, L.; Lenting, C.; Fritzsche, M. B. K. Real-time in situ observations of reaction and transport phenomena during silicate glass corrosion by fluid-cell Raman spectroscopy. *Nat. Mater.* **2019**, *18* (4), 342−348.

(10) Dutta, P. K.; Del Barco, B. Raman spectroscopy of zeolite A: influence of silicon/aluminum ratio. *J. Phys. Chem.* **1988**, *92* (2), 354−357.

(11) Bonino, F.; Lamberti, C.; Bordiga, S. *The Chemistry of Metal−Organic Frameworks: Synthesis, Characterization, and Applications*; Wiley: New York, 2016; Vol. *1*.

(12) Knops-Gerrits, P.-P.; De Vos, D. E.; Feijen, E. J. P.; Jacobs, P. A. Raman spectroscopy on zeolites. *Microporous Mater.* **1997**, *8* (1), 3−17.

(13) Dutta, P. K.; Rao, K. M.; Park, J. Y. Correlation of raman-spectra of zeolites with framework architechture. *J. Phys. Chem.* **1991**, *95* (17), 6654−6656.

(14) Dutta, P. K.; Shieh, D. C.; Puri, M. Raman-spectroscopic study of the synthesis of zeolite-Y. *J. Phys. Chem.* **1987**, *91* (9), 2332−2336.

(15) Matson, D. W.; Sharma, S. K.; Philpotts, J. A. Raman spectra of some tectosilicates and of glasses along the orthoclase-anorthite and nepheline-anorthite joins. *Am. Mineral.* **1986**, *71* (5−6), 694−704.

(16) Dutta, P. K.; Shieh, D. C.; Puri, M. Correlation of framework Raman bands of zeolites with structure. *Zeolites* **1988**, *8* (4), 306−309.

(17) Baertsch, M.; Bornhauser, P.; Calzaferri, G.; Imhof, R. H8Si8O12: A model for the vibrational structure of zeolite A. *J. Phys. Chem.* **1994**, *98* (11), 2817−2831.

(18) Blackwell, C. S. Investigation of zeolite frameworks by vibrational properties. 1. The double-four-ring in group 3 zeolites. *J. Phys. Chem.* **1979**, *83* (25), 3251−3257.

(19) Blackwell, C. S. Investigation of zeolite frameworks by vibrational properties. 2. The double-six-ring in group 4 zeolites. *J. Phys. Chem.* **1979**, *83* (25), 3257−3261.

(20) de Man, A. J. M.; van Santen, R. A. The relation between zeolite framework structure and vibrational spectra. *Zeolites* **1992**, *12* (3), 269−279.

DOI: 10.1021/jacs.9b10346
J. Am. Chem. Soc. 2019, 141, 20318−20324

(21) Smirnov, K. S.; Bougeard, D. Molecular dynamics study of the vibrational spectra of siliceous zeolites built from sodalite cages. *J. Phys. Chem.* **1993**, *97* (37), 9434−9440.
(22) Yu, Y.; Xiong, G.; Li, C.; Xiao, F. S. Characterization of aluminosilicate zeolites by UV Raman spectroscopy. *Microporous Mesoporous Mater.* **2001**, *46* (1), 23−34.
(23) Suzuki, Y.; Wakihara, T.; Kohara, S.; Itabashi, K.; Ogura, M.; Okubo, T. Mechanistic Study on the Synthesis of a Porous Zincosilicate VPI-7 Containing Three-Membered Rings. *J. Phys. Chem. C* **2011**, *115* (2), 443−446.
(24) Wardani, M. K.; Kadja, G. T. M.; Fajar, A. T. N.; Subagjo; Makertihartha, I. G. B. N.; Gunawan, M. L.; Suendo, V.; Mukti, R. R. Highly crystalline mesoporous SSZ-13 zeolite obtained via controlled post-synthetic treatment. *RSC Adv.* **2019**, *9* (1), 77−86.
(25) Mofrad, A. M.; Peixoto, C.; Blumeyer, J.; Liu, J.; Hunt, H. K.; Hammond, K. D. Vibrational Spectroscopy of Sodalite: Theory and Experiments. *J. Phys. Chem. C* **2018**, *122* (43), 24765−24779.
(26) Baerlocher, C.; McCusker, L. B.; Olson, D. H. *Atlas of Zeolite Framework Types*, 6th ed.; Elsevier Science B.V.: Amsterdam, 2007.
(27) Díaz-Cabañas, M.-J.; Barrett, A. P. Synthesis and structure of pure SiO2 chabazite: the SiO2 polymorph with the lowest framework density. *Chem. Commun.* **1998**, No. 17, 1881−1882.
(28) Villaescusa, L. A.; Barrett, P. A.; Camblor, M. A. Calcination of Octadecasil: Fluoride Removal and Symmetry of the Pure SiO2 Host. *Chem. Mater.* **1998**, *10* (12), 3966−3973.
(29) Corma, A.; Puche, M.; Rey, F.; Sankar, G.; Teat, S. J. A Zeolite Structure (ITQ-13) with Three Sets of Medium-Pore Crossing Channels Formed by9- and 10-Rings. *Angew. Chem., Int. Ed.* **2003**, *42* (10), 1156−1159.
(30) Yang, X.; Camblor, M. A.; Lee, Y.; Liu, H.; Olson, D. H. Synthesis and Crystal Structure of As-Synthesized and Calcined Pure Silica Zeolite ITQ-12. *J. Am. Chem. Soc.* **2004**, *126* (33), 10403−10409.
(31) Boal, B. W.; Schmidt, J. E.; Deimund, M. A.; Deem, M. W.; Henling, L. M.; Brand, S. K.; Zones, S. I.; Davis, M. E. Facile Synthesis and Catalysis of Pure-Silica and Heteroatom LTA. *Chem. Mater.* **2015**, *27* (22), 7774−7779.
(32) Moteki, T.; Chaikittisilp, W.; Shimojima, A.; Okubo, T. Silica Sodalite without Occluded Organic Matters by Topotactic Conversion of Lamellar Precursor. *J. Am. Chem. Soc.* **2008**, *130* (47), 15780−15781.
(33) Kresse, G.; Furthmüller, J. Efficient iterative schemes for ab initio total-energy calculations using a plane-wave basis set. *Phys. Rev. B: Condens. Matter Mater. Phys.* **1996**, *54* (16), 11169−11186.
(34) Blöchl, P. E. Projector augmented-wave method. *Phys. Rev. B: Condens. Matter Mater. Phys.* **1994**, *50* (24), 17953−17979.
(35) Kresse, G.; Joubert, D. From ultrasoft pseudopotentials to the projector augmented-wave method. *Phys. Rev. B: Condens. Matter Mater. Phys.* **1999**, *59* (3), 1758−1775.
(36) Perdew, J. P.; Burke, K.; Ernzerhof, M. Generalized Gradient Approximation Made Simple. *Phys. Rev. Lett.* **1996**, *77* (18), 3865−3868.
(37) Momma, K.; Izumi, F. VESTA 3 for three-dimensional visualization of crystal, volumetric and morphology data. *J. Appl. Crystallogr.* **2011**, *44*, 1272−1276.
(38) Labat, F.; Baranek, P.; Domain, C.; Minot, C.; Adamo, C. Density functional theory analysis of the structural and electronic properties of TiO2 rutile and anatase polytypes: Performances of different exchange-correlation functionals. *J. Chem. Phys.* **2007**, *126* (15), 154703.
(39) Grimme, S. Accurate description of van der Waals complexes by density functional theory including empirical corrections. *J. Comput. Chem.* **2004**, *25* (12), 1463−1473.
(40) Sen, P. N.; Thorpe, M. F. Phonons in AX2 glasses: From molecular to band-like modes. *Phys. Rev. B* **1977**, *15* (8), 4030−4038.
(41) Galeener, F. L. Band limits and the vibrational spectra of tetrahedral glasses. *Phys. Rev. B: Condens. Matter Mater. Phys.* **1979**, *19* (8), 4292−4297.

DOI: 10.1021/jacs.9b10346
J. Am. Chem. Soc. 2019, 141, 20318−20324